CrystEngComm

Accepted Manuscript

ROYAL SOCIETY OF CHEMISTRY

www.rsc.org/crystengcomm

Ultra-wideline ^{14}N Solid-State NMR as a Method for Differentiating Polymorphs: Glycine as a Case Study

version 13

Stanislav L. Veinberg,[†] Zachary W. Friedl,[†] Kristopher J. Harris,[†] Luke A. O'Dell[‡] and Robert W. Schurko[†,*]

[†] Department of Chemistry and Biochemistry, University of Windsor, 401 Sunset Avenue, Windsor, N9B 3P4, Ontario, Canada

[‡] Institute for Frontier Materials, Deakin University, Waurn Ponds Campus, Geelong, Victoria 3220, Australia

Author for correspondence:

*E-mail: rschurko@uwindsor.ca
Tel: +1 519 253 3000 ext. 3548
Fax: +1 519 973 7098
Web: http://www.uwindsor.ca/schurko

Abstract

Nitrogen-14 solid-state NMR (SSNMR) is utilized to differentiate three polymorphic forms and a hydrochloride (HCl) salt of the amino acid glycine. The ^{14}N quadrupolar interaction is shown to be very sensitive to variations in the local electric field gradients (EFGs) about the ^{14}N nucleus; hence, differentiation of the samples is accomplished through determination of the quadrupolar parameters C_Q and η_Q, which are obtained from analytical simulations of the ^{14}N SSNMR powder patterns of stationary samples (*i.e.*, static NMR spectra, $\nu_{rot} = 0$ Hz). Additionally, differentiation of the polymorphs is also possible via the measurement of ^{14}N effective transverse relaxation time constants, $T_2^{eff}(^{14}N)$. Plane-wave density functional theory (DFT) calculations, which exploit the periodicity of crystal lattices, are utilized to confirm the experimentally-determined quadrupolar parameters as well as to determine the orientation of the ^{14}N EFG tensors in the molecular frame. Several signal-enhancement techniques are also discussed to help improve the sensitivity of the ^{14}N SSNMR acquisition method, including the use of selective deuteration, the application of the BRoadband Adiabatic INversion Cross-Polarization (BRAIN-CP) technique, and the use of variable-temperature (VT) experiments. Finally, we examine several cases where ^{14}N VT experiments employing Carr-Purcell-Meiboom-Gill (CPMG) refocusing are used to approximate the rotational energy barriers for RNH_3^+ groups.

1. Introduction

Although glycine is the simplest of the standard, naturally occurring amino acids, it has a complex series of solid-state structures. Three distinct polymorphs exist at ambient conditions (*i.e.*, α, β and γ). All forms are zwitterionic in the solid state ($H_3N^+CH_2COO^-$) and polymorphism arises from different modes of hydrogen-bonding (H-bonding) due to the disparate arrangements of the molecules in the unit cell.[1,2] The polymorphs have been studied by numerous spectroscopic techniques, including X-ray diffraction,[3–5] thermodynamic studies,[6,7] and ^{1}H and ^{13}C NMR,[8–12] to name a few. Unfortunately, ^{1}H and ^{13}C SSNMR are not always reliable for differentiating polymorphs, as demonstrated by Taylor and Dybowski in their multinuclear SSNMR of glycine.[10]

Nitrogen SSNMR is capable of detecting the subtle changes in the local nitrogen environments that result from different degrees of hydrogen-bonding in several amino acids and more complicated polypeptide systems.[13–19] Nitrogen has two NMR-active nuclides, ^{14}N (nuclear spin, $I = 1$) and ^{15}N ($I = ½$). ^{15}N NMR is much more prevalent because of the relatively narrow peaks and high resolution chemical shift information it can provide; however, ^{15}N has a very low natural abundance (0.37%), requiring that most samples be isotopically enriched, which may be expensive and synthetically challenging. There are several reports describing the use of ^{15}N SSNMR to investigate polymorphism in amino acids: some groups have reported the use of ^{15}N SSNMR to investigate tautomerism[20,21] and polymorphism[22] in histidine, several others have successfully used ^{15}N SSNMR to investigate polymorphism in fully ^{15}N-labelled biological systems,[17–19] and still others have investigated polymorphs of glycine,[22,23] and glycine bound to a silica surface.[23,24] Although ^{15}N SSNMR spectra are sensitive to the protonation state of the nitrogen atom, this sensitivity is reduced when the compounds have the same charge (as is the

case with polymorphs), in that the nitrogen chemical shifts are very similar and differ only by a few ppm. Nitrogen-14 on the other hand is 99.63% naturally abundant but has a lower gyromagnetic ratio (*i.e.*, $\gamma(^{14}N) = 1.93 \times 10^7$ rad T^{-1} s^{-1} *vs.* $\gamma(^{15}N) = -2.71 \times 10^7$ rad T^{-1} s^{-1}).[25,26] Nitrogen-14 SSNMR is largely avoided because of (i) its low Larmor frequencies, which often require specialized probes and/or tuning equipment, and (ii) the fact that ^{14}N has a nuclear spin of 1 with a moderate ^{14}N quadrupole moment ($eQ = 20.44 \times 10^{-31}$ m^2),[25] which results in inhomogeneously broadened powder patterns that typically span hundreds of kHz to several MHz. This pattern broadening arises from the quadrupolar interaction (QI), which is the interaction between the quadrupolar nucleus (*i.e.*, $I > ½$) and the surrounding EFGs. In particular, the first-order quadrupolar interaction (FOQI) dominates the appearance of ^{14}N SSNMR spectra, and its orientation dependence results in a typical Pake doublet pattern for $I = 1$ nuclei, from which the quadrupolar coupling constant and quadrupolar asymmetry parameter, denoted C_Q, and η_Q, respectively, can easily be determined (see Table 1 for formal definitions). The entire nitrogen chemical shift range spans *ca*. 1300 ppm;[27] hence, the effects of nitrogen chemical shifts, including chemical shift anisotropies (CSAs) are rarely detected in static ultra-wideline (UW) ^{14}N SSNMR spectra (UW NMR spectra are defined as those that must be acquired with specialized techniques such as chirped pulses, stepped transmitters or swept fields, due to limitations in excitation bandwidth associated with conventional rectangular pulses).[28] In cases where the ^{14}N spectra are narrow due to very small quadrupolar coupling constants (*i.e.*, samples with high Platonic symmetry), it is possible to extract both the quadrupolar parameters and the CSA.[29–31] Although it is possible to acquire UW ^{14}N SSNMR spectra under conditions of magic-angle spinning in order to observe the simultaneous effects of the CSA and the first-

and second-order quadrupolar interactions, long acquisition times (*ca*. 44 – 88 hours) and very stable spinning speeds (*i.e.*, specialized probes) are required for such experiments.[13]

For most nitrogen-containing structural motifs, the local bonding environment and symmetry produce large electric field gradients (EFGs) at the ^{14}N nuclei which give rise to large FOQIs, which in turn broaden most ^{14}N NMR powder patterns beyond the excitation bandwidths of most high-power rectangular pulses. Recently, our research group has demonstrated that pulse sequences incorporating broadband frequency-swept pulses can be used to efficiently acquire ^{14}N SSNMR spectra of such systems.[14,15,32] We note that standard rectangular pulses are suitable for cases in which the nitrogen environments have high spherical or Platonic symmetry, and correspondingly small quadrupolar coupling constants and a narrow powder patterns.[33] Frequency-swept Wideband, Uniform Rate, Smooth Truncated (WURST)[34,35] pulses, in conjunction with the Carr-Purcell Meiboom-Gill (CPMG) refocusing protocol,[36] have been demonstrated to be effective for acquiring ^{14}N SSNMR spectra at moderate and high magnetic fields (*i.e.*, 9.4 to 21.1 T).[14–16] However, in many cases, even the broadband excitation afforded by the WURST pulses is not sufficient to completely excite the entire powder pattern in a single experiment. Therefore, ^{14}N SSNMR spectra are often acquired by stepping the transmitter frequency in even increments across the breadth of the powder pattern (this is the so-called variable-offset cumulative spectra (VOCS) method).[37,38] Fortunately, given the symmetric nature of the ^{14}N Pake doublet powder patterns to first order, it is possible to reduce experimental time by acquiring only half of the ^{14}N powder pattern (and constructing the other half by reflection, if desired; see the experimental section for details).[15,39] For an account of the progress in ^{14}N SSNMR, we refer the readers to a review article published in 2011 by O'Dell L. A.[16]

In this work, we demonstrate that UW ^{14}N SSNMR can be used to differentiate between three polymorphic forms of glycine (*i.e.*, α, β and γ), as well as an HCl salt derivative. Although α-glycine has previously been studied by ^{14}N SSNMR by our group[14,40] and others,[13,41,42] its ^{14}N SSNMR spectra can be acquired with great rapidity, making it useful for comparison to its known polymorphs and salts. We also demonstrate that the polymorphs may be differentiated via the measurement of the effective ^{14}N transverse relaxation time constant, $T_2^{eff}(^{14}N)$. The ^{14}N EFG tensor parameters of the polymorphic phases are correlated to their crystal structures *via* the use of plane-wave DFT calculations. We also discuss how the unique structural and dynamical properties of the RNH_3^+ moieties, which are common in many nitrogen-containing compounds, can be exploited to enhance S/N, improve spectral quality, and reduce experimental times. The sensitivity of ^{14}N SSNMR may prove particularly useful for the study of more industrially interesting systems such as active pharmaceutical ingredients (APIs) and other organic and inorganic molecules of interest.

2. Experimental Methods

2.1 Sample preparation. Samples of α-glycine, γ-glycine, and glycine HCl were obtained from Sigma Aldrich and used without further purification. High purity samples of β-glycine were prepared by the method described by Boldyreva *et al.*[1] A deuterated sample of γ-glycine was prepared by the method described by Harris *et al.*[43] The phase purities of all samples were confirmed by powder X-ray Diffraction (pXRD) (Fig. S1, Supplementary Information).

2.2 Powder XRD experiments. Diffraction patterns for all the samples were collected using a D8 DISCOVER X-ray diffractometer equipped with an Oxford Cryosystems 700 Cryostream Plus Cooler. A Cu-K_α (λ = 1.54056 Å) radiation source with a Bruker AXS HI-STAR area detector running under the General Area Detector Diffraction Systems (GADDS) were used. Powder patterns were simulated with the PowderCell software package.[44]

2.3 Direct-Excitation (DE) NMR experiments. All spectra were acquired using a Varian InfinityPlus spectrometer equipped with a wide-bore 9.4 T magnet using Larmor frequencies of 399.73 MHz and 28.875 MHz for ^{1}H and ^{14}N, respectively. A Chemagnetics 5.0 mm static double-resonance HX probe was used for all experiments, equipped with a Varian/Chemagnetics low-γ tuning box on the ^{14}N channel. Spectra were referenced against a sample of solid NH_4Cl (δ_{iso} = 39.3 ppm),[45] although chemical shifts are not reported due to large uncertainties in their measurements (*vide infra*).

Due to the large breadths of the ^{14}N NMR powder patterns, the WURST-CPMG pulse sequence[46] was used for DE ^{14}N NMR experiments, as previously described elsewhere.[16,38,20] WURST-80[34] pulses 50 μs in length were linearly swept from low to high frequency covering a total range of 2 MHz and with a maximum amplitude of ν_1 = 30 kHz. Continuous wave (CW)

^{1}H decoupling with ν_2 = 40 kHz was applied during the duration of each scan.[14,48] With our current low-γ probe circuit configuration, we are restricted to an upper maximum of *ca*. 40 kHz for proton decoupling power, which means that for some samples it is not possible to fully decouple the ^{14}N-^{1}H heteronuclear dipolar interactions.

Individual sub-spectra were acquired at evenly-spaced transmitter frequencies, which were chosen such that (i) they are integer multiples of the CPMG spikelet spacing, and (ii) the overlap between the individual sub-spectra is optimized to yield undistorted spectra.[39] Each sub-spectrum was zero-filled, apodized, Fourier transformed, and magnitude processed. Only the high-frequency sides of the ^{14}N powder patterns were acquired, with the low frequency sides of the patterns produced by reflection (since the ^{14}N Pake doublet is symmetric about the isotropic chemical shift to first order).[15,16] Table S1 (Supporting Information) shows a complete list of acquisition parameters. ^{14}N SSNMR powder patterns were simulated using the WSolids1 program.[49]

2.4 Variable-Temperature (VT) NMR experiments. ^{14}N WURST-CPMG spectra of non-deuterated α- and γ-glycine were acquired at multiple temperatures ranging from −88 °C to +181 °C with a Varian VT upper stack and nitrogen gas heat exchanger. Temperatures were calibrated using the ^{207}Pb isotropic shift of solid $Pb(NO_3)$, as suggested by Bielecki and Burum.[50] We refer the readers to Tables S2 and S3 for detailed lists of temperatures and acquisition parameters.

2.5 BRoadband Adiabatic Inversion Cross-Polarization (BRAIN-CP) NMR experiments. A ^{14}N SSNMR spectrum of glycine HCl was acquired using the BRAIN-CP/WCPMG[51] pulse sequence in order to compare the performances of DE and cross-polarization (CP) pulse sequences. The frequency sweep range of the X-channel (X = ^{14}N) contact pulse was set to ensure that abundant ^{1}H spin-polarization was transferred predominantly

to the +1 → 0 fundamental transition.[40] A 16-step phase cycle was employed to remove zero-quantum coherences (arising from thermal polarization) so that the WCPMG refocusing pulses only refocused the polarization resulting from the CP process.[40] For a complete list of experimental parameters, please refer to Tables S4 and S5.

2.6 Ab initio calculations. Plane-wave density functional theory (DFT) calculations of the ^{14}N EFG tensors were performed using the CASTEP NMR program[52] in the Materials Studio 5.0 software suite on a Dell Studio XPS 435T/9000 with a single Intel Core i7 920 processor and 8 GB of DDR3 RAM. "On the fly" ^{14}N pseudopotentials were used for these calculations, with a plane-wave basis set cut-off of 610 eV and a fine *k*-point set (2 x 2 x 4). The revised Perdew, Burke and Ernzerhof (rPBE) functional was used in the generalized gradient approximation (GGA) for the exchange correlation energy. For all of the crystal structures, geometry optimizations of the hydrogen atom positions were carried out, while holding fixed the positions of all other heavier atoms and lattice parameters. Crystal structures for α-glycine, β-glycine, γ-glycine, and glycine HCl were obtained from the Cambridge Structural Database (CSD).[4,53–55]

3. Results and Discussion

3.1 ^{14}N SSNMR spectra of the different forms of glycine: direct-excitation experiments.

In this section, a brief discussion of the ^{14}N SSNMR spectra of the various forms of glycine is presented. In all cases, the S/N ratio for each spectrum is high enough that two of the three discontinuities associated with the principal components of the ^{14}N EFG tensor can be observed. The outermost discontinuities, which correspond to the largest component of the EFG tensor, V_{33}, are hard to clearly discern in certain cases. Fortunately, only two of the three discontinuities need to be resolved to accurately obtain the quadrupolar parameters (this is because the EFG tensor is traceless, *i.e.*, $V_{33} = -(V_{11} + V_{22})$.[16] Due to variations in the longitudinal relaxation time constant, $T_1(^{14}\text{N})$, and the effective transverse relaxation time constant, $T_2^{\text{eff}}(^{14}\text{N})$, the acquisition times vary for each sample (*vide infra*). We note that the terminology "effective $T_2(^{14}\text{N})$" or "$T_2^{\text{eff}}(^{14}\text{N})$" is used to describe transverse relaxation, due to the partial or complete absence of contributions to relaxation from ^{14}N-^{1}H dipolar coupling resulting from the application of high-power ^{1}H decoupling. Table 1 shows the values of C_Q, η_Q, and $T_2^{\text{eff}}(^{14}\text{N})$ at room temperature (*i.e.*, 20 ^{o}C) for the aforementioned compounds.

3.1.1 α-, β-, and γ-glycine. The ^{14}N NMR powder pattern for α-glycine (Fig. 1a) has high S/N, and the discontinuities arising from all three principal axes of the EFG tensor are clearly visible. Analytical simulation of this spectrum yields $C_Q = 1.19 \pm 0.02$ MHz and $\eta_Q = 0.52 \pm 0.02$, in close agreement with previously obtained results.[13,14] The ^{14}N NMR powder pattern for β-glycine (Fig. 1b) also has high S/N, although it required a significantly longer acquisition time than that of α-glycine (*i.e.*, *ca*. 7.6 hours for the former vs. 0.5 hours for the latter). Comparing the free induction decays (FIDs), which were acquired with identical ^{1}H decoupling fields, reveals that the ^{14}N nuclei in β-glycine have a shorter $T_2^{\text{eff}}(^{14}\text{N})$ value than

those in α-glycine, resulting in the collection of fewer spin echoes and thereby necessitating a larger number of scans to obtain a spectrum with comparable S/N (see Table S1). A more detailed discussion of the measurement of $T_2^{eff}(^{14}N)$ is presented below.

The discontinuities in the spectrum of β-glycine are distinct from those in the spectrum of α-glycine, indicating that each sample is characterized by a unique set of quadrupolar parameters. Indeed, analytical simulation of the spectrum of β-glycine yields $C_Q = 1.26 \pm 0.03$ MHz and $\eta_Q = 0.42 \pm 0.03$. The ^{14}N NMR spectrum for the third polymorph, γ-glycine, is shown in Fig. 1c. During acquisition of the sub-spectra of γ-glycine, acoustic ringing was observed in the FIDs (Fig. S2). The acoustic ringing likely arises from the piezoelectric nature of this sample, as described in previous publications.[5,56–61] Due to the semi-coherent nature of the ringing, its distorting effect can eventually be reduced with the use of signal averaging (complete averaging requires a large number of scans). Nonetheless, the "horn" and "shoulder" discontinuities are still clearly resolved, and analytical simulations of the powder pattern yield $C_Q = 1.19 \pm 0.04$ MHz and $\eta_Q = 0.38 \pm 0.04$. Although the value of C_Q is the same as that of α-glycine, the powder patterns are distinct in terms of the locations of the "horn" and "shoulder" discontinuities arising from their different η_Q values. Similar to the observation made for β-glycine, the FIDs of γ-glycine are associated with $T_2^{eff}(^{14}N)$ values that differ from those observed for both α- and β-glycine (*vide infra*).

The $T_2^{eff}(^{14}N)$ constants can be measured by fitting the CPMG echo trains with a first-order exponential decay function; however, we note that the $T_2^{eff}(^{14}N)$ values must be measured for individual sub-spectra (*i.e.*, from FIDs acquired at single transmitter frequencies). For a transmitter frequency of 29.175 MHz, and a ^1H decoupling field of $\nu_2 = 40$ kHz, the $T_2^{eff}(^{14}N)$ values are measured to be 54 ± 14, 12 ± 0.6, and 25 ± 3.7 ms for α-, β-, and γ-glycine,

respectively (Fig. S3). The $T_2^{eff}(^{14}N)$ constant for the β-glycine sample is the shortest (corresponding to the most rapid decay of the echo train), suggesting that there are larger contributions to transverse relaxation from heteronuclear ^{14}N-^{1}H dipolar couplings than in the cases of the α- and γ-glycine samples. This assumption is reasonable, since the values of C_Q are similar for all three compounds, meaning that it is unlikely to be much variation in the quadrupolar contributions to transverse relaxation. An interesting implication of this result is that it may be possible to differentiate polymorphs of some samples solely on the basis of the T_2 relaxation characteristics without having to acquire the entire ^{14}N powder pattern, which may be of use for discriminating systems which possess similar quadrupolar parameters, or possess ^{14}N patterns that are simply too broad to acquire in their entirety.

3.1.2 Glycine HCl. Although glycine HCl is a distinct chemical compound, it is of interest to see whether its ^{14}N quadrupolar parameters differ from those of the free-base glycine polymorphs. This of course could have great relevance in the characterization and differentiation of a variety of organic free-base compounds and their corresponding HCl salts, including amino acids, pharmaceuticals and numerous other systems. The ^{14}N NMR powder pattern for glycine HCl (Fig. 1d) has comparable S/N to the powder pattern of α-glycine, with all of the discontinuities clearly resolved. The slightly lower signal intensity of the glycine HCl spectrum compared to that of α-glycine mainly arises from the shorter CPMG echo train (*i.e.*, shorter $T_2^{eff}(^{14}N)$, Table 1) of the former. The quadrupolar parameters are $C_Q = 1.16 \pm 0.02$ MHz and $\eta_Q = 0.17 \pm 0.02$. Again, C_Q is very similar to that of α- and γ-glycine; however, its distinct η_Q value leads to a powder pattern that is easily distinguishable.

3.1.3 Correlation of ^{14}N NMR data to molecular structure. All of the ^{14}N NMR spectra presented above are associated with pseudo-tetrahedral nitrogen environments (*i.e.*, RNH_3^+,

where R denotes the rest of the amino acid). In an idealized "gas phase" system, this moiety most often possesses a C_3 rotation axis along the C-N bond, which results in an axially symmetric ^{14}N EFG tensor ($\eta_Q = 0$) with the principal component of largest absolute magnitude, V_{33}, aligned directly along this axis. However, the systems studied herein do not possess perfect C_3 rotational axes due to intermolecular interactions in the solid state involving the NH_3 group (*i.e.*, hydrogen bonding); hence, the ^{14}N EFG tensors do not have perfect axial symmetry (*i.e.*, $V_{11} \neq V_{22}$ and $\eta_Q \neq 0$). In every case, the V_{33} component is still expected to align along, or close to, the direction of the C-N bond.

Plane-wave DFT calculations have been carried out to correlate the local structures of the nitrogen environments with experimentally-obtained ^{14}N quadrupolar parameters (Table 1). Plane-wave calculations are suitable for crystalline systems where intermolecular interactions may influence the EFG tensor components and orientations, since the extended crystal lattice is taken into account.[14,62,63] In all of the cases examined herein, the theoretically predicted ^{14}N quadrupolar parameters closely match the experimental data. For the structure obtained using an X-ray source (*i.e.*, β-glycine[4]), the prediction of quadrupolar parameters is improved if the EFG calculations are conducted after the proton positions have been optimized (the positions of the heavier atoms and lattice parameters were held constant). For structures obtained using a neutron source (*i.e.*, α-glycine,[53] γ-glycine,[54] and glycine HCl[55]), the values of C_Q and η_Q are predicted accurately whether or not the proton positions are geometry optimized.

The theoretically predicted ^{14}N EFG tensor orientations for all four systems are shown in Fig. 2. In each case, V_{33} is oriented nearly along the C-N bond, as discussed above. In all cases, the sign of C_Q is predicted to be positive (Table 1), as expected.[15,64] Although the sign of C_Q cannot be determined experimentally from ^{14}N SSNMR spectra, it has been measured to be

positive from the measurement of ^{13}C-^{14}N residual dipolar couplings in the ^{13}C SSNMR spectrum of α-glycine,[65] as well as from ^{14}N nuclear quadrupole resonance (NQR) experiments of other crystalline amino acids.[66,67]

In order to correlate the calculation results to known crystal structures, we restrict our discussion to α-glycine, γ-glycine, and glycine HCl. If one considers the lengths of the N-H bonds in the three samples (Table S6), it is evident that glycine HCl has the shortest N-H bonds (*i.e.*, all of the N-H bonds are < 1.4 Å), suggesting that the amount of hydrogen-bonding with neighbouring molecules is very limited, resulting in a nearly axially symmetric EFG tensor (*i.e.*, $\eta_Q \approx 0$). Both α- and γ-glycine have one or more N-H bonds that are clearly affected by H-bonding (*i.e.*, N-H bond length > 1.5 Å), thereby resulting in an EFG tensor that is less axially symmetric with an intermediate η_Q value (*i.e.*, $\eta_Q \approx 0.5$).

Finally, some brief comments must be made on motional effects on the ^{14}N EFG tensors. This has been recently studied in a number of ^{14}N SSNMR experiments on a variety of different structural moieties.[14,48,68] Despite the fact that NH_3 groups are known to undergo a three-fold-jump motion about the C-N bond in the solid state,[69–71] the magnitude of V_{33} should not be substantially influenced by the motion, since V_{33} is oriented along or near the C-N bond. In addition, V_{11} and V_{22} do not shown any evidence of averaging due to the motion, even at higher temperatures where rotational rates are expected to increase (*vide infra*).

3.2 Improving the efficiency of ^{14}N SSNMR experiments. The two NMR interactions that make the most significant contributions to nuclear magnetic relaxation processes in ^{14}N SSNMR experiments are the ^{14}N quadrupolar and ^{14}N-^{1}H direct dipolar interactions. Due to the strong dipolar couplings that arise from the short N-H bonds, both the longitudinal and transverse relaxation times are expected to be dominated by the ^{14}N-^{1}H dipolar coupling mechanism, the latter results in short CPMG echo trains and reduced S/N. Ideally, it is desirable to acquire ^{14}N CPMG NMR spectra of such systems with as high a ^{1}H decoupling power as possible, in order to maximize the effective $T_2(^{14}N)$ (*vide supra*). We remind the reader that with the low-γ configuration of our probe, the ^{1}H decoupling rf is limited to a maximum of *ca*. 40 kHz. It is noted that during the course of this study, we have investigated a variety of schemes to increase the efficiency of ^{1}H decoupling; however, no one decoupling scheme has been found to be more efficient (a full discussion of ^{1}H decoupling and the impacts on UW NMR experiments is beyond the scope of the current work, and further work on this issue is currently underway in our laboratory).

Since we cannot resort to simply using the highest ^{1}H decoupling fields possible as the sole means of acquiring higher quality ^{14}N SSNMR spectra, alternatives must be considered. Hence, in this section, we discuss several techniques that improve the efficiency of ^{14}N UW SSNMR experiments by increasing the S/N ratio and the spectral quality through the combined use of high-power ^{1}H decoupling, deuteration, broadband cross-polarization (BCP), and VT NMR.

3.2.1 ^{1}H decoupling and deuteration. By using CW ^{1}H decoupling to attenuate or eliminate the impact of relaxation arising from heteronuclear ^{14}N-^{1}H dipolar coupling during the acquisition of a ^{14}N FID, the number of spin echoes that form (and thus the resulting S/N of the

Fourier-transformed spectrum) can be controlled (Fig. S4). As described in previous works, the more spin echoes that compose a CPMG echo train, the higher the S/N of the resulting spectrum.[72–74] An alternative to using high-power ^{1}H decoupling to average heteronuclear ^{14}N-^{1}H dipolar couplings is to recrystallize the amino acids from an exchanging deuterated solvent (*e.g.*, D_2O). Exchanging nitrogen-bound protons for deuterons can decrease or eliminate (depending on the degree of exchange) the contribution of the ^{14}N-^{1}H dipolar coupling mechanism to the T_2 relaxation of the ^{14}N nucleus,[14] since the gyromagnetic ratio of ^{2}H is significantly lower than that of ^{1}H ($\gamma_{2H} = 4.1 \times 10^7$ rad T^{-1} s^{-1} *vs.* $\gamma_{1H} = 26.7 \times 10^7$ rad T^{-1} s^{-1}). We note that due to the non-trivial synthesis of β-glycine, the instability of its solid form, and several failed attempts to deuterate the sample, the effects of deuterium labelling were not studied for the β-glycine polymorph. In addition, all of our attempts to recrystallize α-glycine from D_2O (*l*) have resulted in the formation of γ-glycine-ND_3^+.

Fig. 3 provides a comparison of the ^{14}N powder patterns of γ-glycine-ND_3^+ and its non-deuterated counterpart, γ-glycine. The powder pattern of γ-glycine-ND_3^+ (Fig. 3a) has the appearance of a nearly ideal ^{14}N SSNMR spectrum, with discontinuities that are very well-defined, especially in the "foot" region. The corresponding analytical simulation is the red trace in Fig. 3. The quadrupolar parameters are $C_Q = 1.19 \pm 0.02$ MHz and $\eta_Q = 0.37 \pm 0.02$ and have smaller uncertainties compared to those of the non-deuterated sample of γ-glycine (*vide supra*). We note that even with deuteration, proton decoupling is still required to obtain high quality spectra, since other nearby protons (which do not exchange) can impact the transverse relaxation and therefore reduce the number of spin echoes that form in the CPMG echo train. Measurement of the $T_2^{eff}(^{14}N)$ constant in the sample of γ-glycine-ND_3^+ yielded 24 ± 3 ms, which within the level of uncertainty is equal to the T_2^{eff} value of the non-deuterated γ-glycine polymorph (T_2^{eff} =

25 ± 4 ms). As a result, the overall S/N of the spectrum is comparable to that observed for γ-glycine. The comparable $T_2^{eff}(^{14}N)$ value for the deuterated sample is a puzzling result, since it contradicts previous findings which show that deuteration of a nitrogen environment often increases the $T_2^{eff}(^{14}N)$ time constant.[14,16,40] It is possible that ^{14}N-^{1}H dipolar coupling involving the proximate CH_2 protons makes a major contribution to the $T_2^{eff}(^{14}N)$; this could be due to the rapid rotational motion of the NH_3 group (*vide infra*). However, this is unlikely because comparison of ^{14}N SSNMR sub-spectra for α-glycine and α-glycine-D_5 reveals that their $T_2^{eff}(^{14}N)$ values are the same within uncertainty (Fig. S5). Interestingly, no ringing was observed in the FID of γ-glycine-ND_3^+, unlike the corresponding FID of non-deuterated γ-glycine (Fig. S2). We are currently investigating this phenomenon in greater detail.

3.2.2 Broadband Cross-Polarization (BCP). Our group has recently published work demonstrating the ability of using cross-polarization over a broad frequency range.[40,51,75] The use of the BRoadband Adiabatic INversion Cross-Polarization (BRAIN-CP) pulse sequence provides all the advantages of regular CP experiments (*i.e.*, enhancement based on the ratio of the γ's, recycle delays that depend on the $T_1(^{1}H)$ constants, etc.), as well as the added benefit of a broad CP excitation profile, all of which lead to decreased experimental times.[21] The benefits of BRAIN-CP for ^{14}N SSNMR have previously been demonstrated by our group with the use of a sample of α-glycine and several pharmaceutical compounds.[40] In fact, α-glycine is an excellent ^{14}N NMR setup standard for both direct-excitation and CP experiments. We have investigated the effectiveness of BRAIN-CP for the acquisition of ^{14}N SSNMR spectra of β-glycine, γ-glycine and glycine HCl.

Fig. 4a shows a comparison of individual sub-spectra of glycine HCl acquired with WURST-CPMG[46] and BRAIN-CP/WURST-CPMG[51] at the same transmitter frequency. For

brevity, these direct-excitation and broadband cross-polarization experiments will be referred to as DE and BCP, respectively. The DE and BCP experiments were conducted with almost identical parameters, including the overall number of scans. The BCP sub-spectrum acquired at a transmitter frequency of 29.225 MHz has approximately 6.5 times the S/N of the corresponding DE sub-spectrum. Fig. 4b shows a comparison of the ^{14}N powder patterns of glycine HCl acquired with both BCP and DE. It is evident that under the same experimental conditions, the signal intensity of the BCP spectrum is far better than that of the DE spectrum; in particular, the outer "foot" discontinuity is clearly visible in the BCP spectrum.

BCP experiments were also attempted on both β- and γ-glycine; however, they were unsuccessful. This could be due to several factors including poor CP transfer efficiency, short $T_{1\rho}$'s (both ^{1}H and ^{14}N) of the samples, efficient cross-relaxation, etc. We attempted ^{1}H-^{14}N BCP experiments on γ-glycine at a higher temperature (*i.e.*, T_{max} = 92 °C, *vide infra*) in order to see if the CP process differs with changes in the dynamical motions of the NH_3 moieties; however, spectra of adequate S/N could still not be obtained. It is clearly of interest to continue investigating the dependence of the CP mechanism on ^{1}H-^{14}N cross relaxation and the motion of the RNH_3^+ moieties (*vide infra*), since this may enable the use of BCP experiments for a wider range of samples and different modes of polymorph differentiation; however, detailed investigation of these factors is beyond the scope of the current work.

In cases where BCP experiments can be conducted and the CP conditions are favourable, high S/N spectra may be acquired in shorter experimental times than their DE counterparts. A second advantage of using BRAIN-CP to acquire ^{14}N SSNMR powder patterns is that due to the added S/N that results in many cases, ^{14}N powder patterns with high C_Q values (*i.e.*, C_Q > 1.6 MHz) may now be acquired at moderate magnetic field strengths (*i.e.*, 9.4 T), a practice which,

to the best of our knowledge, has been limited to ultrahigh-field NMR (*i.e.*, 21.1 T),[15,16] ^{14}N overtone spectroscopy,[76–79] single-crystal NMR,[80] and NQR.[81–88]

3.2.3 Variable-temperature (VT) ^{14}N NMR experiments. One of the factors that influences the sensitivity of NMR experiments is temperature. The most obvious influence of temperature is the enhancement of S/N which is generally observed for spectra acquired at lower temperatures, due to modifications of the spin populations described by the Boltzmann equation. However, motional effects on relaxation can have a major impact on S/N and resolution. For instance, it has been shown that for a methyl group that undergoes rotational motions (*i.e.*, three-fold rotation) in the solid state, the relaxation characteristics of the ^{1}H and ^{13}C nuclides (*i.e.*, T_1's and T_2's) can be altered by changing the temperature.[89] Exploiting temperature-dependent relaxation characteristics can result in decreased experimental times and/or lend insight into dynamical processes at the molecular level.[48,68,90–93] In this section, we briefly discuss the effect of variation in temperature on the acquisition of ^{14}N SSNMR powder patterns; this was achieved with a series of sub-spectra of α-glycine, γ-glycine, and glycine HCl acquired at temperatures ranging from −88 °C to +181 °C. We note that due to the unstable nature of β-glycine, VT ^{14}N SSNMR experiments were not attempted for this sample.

For α-glycine (Fig. 5a), we observed that the ^{14}N sub-spectrum with maximum S/N occurs at a sample temperature of *ca*. 20 °C, with the S/N decreasing as the temperature is ramped away from 20 °C in either direction. For the rest of our discussion, we introduce the variable T_{max} to denote the *sample temperature at which we observe the maximum S/N ratio*. For γ-glycine (Fig. 5b), we note that $T_{max} \approx 92$ °C, and the S/N appears to be roughly 25% higher than the room temperature (*i.e.*, 20 °C) sub-spectrum. For glycine HCl (Fig. 5c), we found that $T_{max} \approx 2$ °C. Since the S/N of ^{14}N WCPMG SSNMR powder patterns is largely dependent on

the $T_2^{eff}(^{14}N)$, it is clear that the variation of temperature serves to shorten or lengthen $T_2^{eff}(^{14}N)$, resulting in fewer or more spin echoes, respectively, in the CPMG echo train (Fig. S6). The behaviour of the ^{14}N echo trains throughout the temperature range suggests that the ^{14}N-^{1}H dipolar coupling mechanism is likely a combination of two components: a static component (secular) and a dynamic component (non-secular). Using α-glycine as an example (Fig. 5a), as the temperature is decreased below T_{max} = 20 °C (*e.g.*, T = −43 °C), the rotational rate of the NH_3 group is decreased and the secular component dominates the relaxation. Conversely, if the temperature is increased above T_{max} (*e.g.*, T = 92 °C), the NH_3 group rotates at a more rapid rate and the non-secular component dominates the relaxation. At T_{max}, neither relaxation mechanism is overly dominant, resulting in the most inefficient (longest) $T_2^{eff}(^{14}N)$ relaxation, and accordingly, the highest S/N in the corresponding CPMG spectra.

The rotational motion of NH_3 groups of solid amino acids has been investigated with both ^{1}H and ^{2}H SSNMR; in some cases, it is possible to calculate the rotational activation barriers for this motion based on NMR measurements.[43,69,71] The rotational motion is described as a three-fold-jump; the barrier to this rotation is given by the Arrhenius equation for a single-energy activation model:[70,92]

$$\tau_c = \tau_o e^{\left(\frac{E_A}{RT}\right)} \quad [1]$$

where τ_c is the correlation time, τ_o is the pre-exponential factor (infinite-temperature correlation time), E_A is the rotational barrier energy, R is the gas constant, and T is the temperature. The rotational barrier for α-glycine has been previously calculated to be 21.7 kJ mol^{-1},[10] while the rotational barrier for γ-glycine has been measured as 28.6 kJ mol^{-1}.[12] Based on these known activation energies and a τ_o value which is equal to 0.7×10^{-14} s,[10,12] the correlation times, τ_c, at room temperature (*i.e.*, 20 °C) are calculated to be 0.05 ns and 0.87 ns for α- and γ-glycine,

respectively. The correlation times at T_{max} for α- and γ-glycine are calculated to be 0.05 ns and 0.08 ns, respectively. Thus, it would appear that at T_{max}, the correlation times for the two samples become similar, further suggesting that the rate at which the NH_3 group is rotating causes variation in the $T_2^{eff}(^{14}N)$.

To the best of our knowledge, the NH_3 rotational barrier of glycine HCl has not been reported in the literature. From our ^{14}N VT SSNMR experiments, with the use of finer temperature steps in the range of −16 °C to 20 °C (Fig. S7), we have observed that T_{max} is approximately −11 °C (unlike the 2 °C which we observed with a coarser temperature increment, Fig. 5c). By assuming that the correlation time of the NH_3 rotation would have to be similar, or equivalent, to that of α-glycine (*i.e.*, $\tau_c = 0.05$ ns), and keeping τ_o equivalent to that of α-glycine ($\tau_o = 0.7 \times 10^{-14}$ s for α-glycine and γ-glycine),[10,12] the rotational barrier for the NH_3 group in glycine HCl is calculated to be 19.4 kJ mol^{-1}.

Full ^{14}N SSNMR spectra of both α-glycine and γ-glycine were acquired at room temperature (*i.e.*, 20 °C) as well as an alternate temperature (*i.e.*, −43 and 92 °C for α-glycine and γ-glycine, respectively) and the quadrupolar parameters remain unchanged (Fig. S8). The invariance of the quadrupolar parameters within the investigated temperature range can be attributed to the geometry of the nitrogen moiety, as discussed above (again, we note that drastic changes in η_Q would be indicative of a major structural change and/or phase transition). While the measurement of $T_2^{eff}(^{14}N)$ constants gives insight into rotational barriers and rates of motion, it may also serve to enable differentiation of subtly different polymorphic forms, or perhaps the discovery of new polymorphs, on the basis of disparate $T_2^{eff}(^{14}N)$ constants over a wide range of temperatures.

4. Conclusions:

In this work, we have demonstrated the effectiveness of ^{14}N SSNMR for differentiating between polymorphic forms of glycine, as well as its HCl salt derivative. Differentiation is achieved by determining and comparing the quadrupolar parameters, C_Q and η_Q, without the need for chemical shift information. We note that differentiating the various forms of glycine can be achieved by comparing not only their respective quadrupolar parameters, but also by comparing their $T_2^{eff}(^{14}N)$ constants. Since this methodology could be used for a wide range of organic solids which feature RNH_3 moieties, including solids which may be disordered and unamenable to characterization via X-ray methods, we have also discussed several methods for improving the acquisition of ^{14}N SSNMR powder patterns. High-power ^{1}H decoupling is an effective means of increasing S/N; however, the limit to what power can be used depends upon the hardware available and the nature of the samples being investigated. Hence, ^{1}H decoupling is best utilized with any or a combination of RNH_3 group deuteration and variable temperature acquisition (for minimization of $T_2^{eff}(^{14}N)$ and maximization of S/N), as well as broadband CP (where appropriate). We have also briefly highlighted the dynamical motion of the NH_3 group and its variation with temperature, and how this impacts S/N in ^{14}N CPMG and ^{1}H-^{14}N CP NMR spectra. More work is needed to clearly elucidate the relaxation mechanisms at play in both of these cases. In addition, we have utilized plane-wave DFT calculations to accurately predict the ^{14}N EFG tensor components by taking into account the periodic nature exhibited by crystals.

We hope that this work inspires other researchers to utilize ^{14}N SSNMR as an additional tool in their spectroscopic toolbox for the study of nitrogen-containing systems of varying complexity. One such area that has immense potential that we are currently investigating is polymorph differentiation of nitrogen-containing HCl pharmaceutical compounds. It is clear that

the sets of different secular and non-secular ^{14}N NMR parameters that can be measured with relatively ease should be very useful for polymorph recognition and discovery, the identification of impurity phases or phase transitions, and perhaps even the differentiation of distinct chemical forms of both crystalline and amorphous pharmaceuticals, including free-base organic molecules, organic salts and co-crystalline species.

5. Acknowledgements:

R.W.S. thanks NSERC for funding this research in the form of a Discovery Grant and Discovery Accelerator Supplement. R.W.S. is also grateful for an Early Researcher Award from the Ontario Ministry of Research and Innovation. S.L.V. thanks the province of Ontario for a Queen Elizabeth II – Graduate Scholarship in Science and Technology as well as an Ontario Graduate Scholarship. We are also grateful for the funding of the Laboratories for Solid-State Characterization at the University of Windsor from the Canadian Foundation for Innovation, the Ontario Innovation Trust, and the University of Windsor. This work was made possible, in part, by the facilities of the Shared Hierarchical Academic Research Computing Network (SHARCNET: www.sharcnet.ca).

Bibliography

1 V. A. Drebushchak, Y. A. Kovalevskaya, I. E. Paukov and E. V. Boldyreva, *J. Therm. Anal. Calorim.*, 2003, **74**, 109–120.

2 V. M. Kozhin, *Kristallografiya*, 1978, **23**, 1211–1215.

3 L. F. Power, K. E. Turner and F. H. Moore, *Acta Crystallogr. Sect. B-Structural Sci.*, 1976, **32**, 11–16.

4 T. N. Drebushchak, E. V. Boldyreva and E. S. Shutova, *Acta Crystallogr. Sect. E*, 2002, **58**, O634–O636.

5 Y. Iitaka, *Acta Crystallogr.*, 1961, **14**, 1–10.

6 E. V. Boldyreva, V. A. Drebushchak and T. N. Drebushchak, *J. Therm. Anal. Calorim.*, 2003, **73**, 409–418.

7 E. V. Boldyreva, V. A. Drebushchak and T. N. Drebushchak, *J. Therm. Anal. Calorim.*, 2003, **73**, 419–428.

8 R. E. Taylor, *Conc. Magn. Reson.*, 2004, **22A**, 79–89.

9 I. V. Drebushchak, S. G. Kozlova, A. R. Semenov and E. V. Boldyreva, *J. Mol. Struct.*, 2008, **885**, 176–178.

10 R. E. Taylor and C. Dybowski, *J. Mol. Struct.*, 2008, **889**, 376–382.

11 K. Yamada, T. Shimizu, T. Yamazaki and A. Sato, *Chem. Lett.*, 2008, **37**, 472–473.

12 E. R. Andrew, W. S. Hinshaw, M. G. Hutchins and R. O. I. Sjöblom, *Mol. Phys.*, 1976, **31**, 1479–1488.

13 T. Giavani, H. Bildsøe, J. Skibsted and H. J. Jakobsen, *J. Magn. Reson.*, 2004, **166**, 262–272.

14 L. A. O'Dell and R. W. Schurko, *Phys. Chem. Chem. Phys.*, 2009, **11**, 7069–7077.

15 L. A. O'Dell, R. W. Schurko, K. J. Harris, J. Autschbach and C. I. Ratcliffe, *J. Am. Chem. Soc.*, 2011, **133**, 527–46.

16 L. A. O'Dell, *Prog. Nucl. Magn. Reson. Spectrosc.*, 2011, **59**, 295–318.

17 A. Dos, V. Schimming, S. Tosoni and H.-H. Limbach, *J. Phys. Chem. B*, 2008, **112**, 15604–15.

18 D. C. Apperley, A. F. Markwell, R. K. Harris and P. Hodgkinson, *Magn. Reson. Chem.*, 2012, **50**, 680–90.

19 H. L. F. Schmidt, L. J. Sperling, Y. G. Gao, B. J. Wylie, J. M. Boettcher, S. R. Wilson and C. M. Rienstra, *J. Phys. Chem. B*, 2007, **111**, 14362–9.

20 S. Li and M. Hong, *J. Am. Chem. Soc.*, 2011, **133**, 1534–44.

21 E. Kolehmainen and B. Ośmiałowski, *Int. Rev. Phys. Chem.*, 2012, **31**, 567–629.

22 H. Kimura, K. Nakamura, A. Eguchi, H. Sugisawa, K. Deguchi, K. Ebisawa, E. I. Suzuki and A. Shoji, *J. Mol. Struct.*, 1998, **447**, 247–255.

23 I. Lopes, L. Piao, L. Stievano and J. F. Lambert, *J. Phys. Chem. C*, 2009, **113**, 18163–18172.

24 I. Ben Shir, S. Kababya and A. Schmidt, *J. Phys. Chem. C*, 2012, **116**, 9691–9702.

25 P. Pyykkö, *Mol. Phys.*, 2001, **99**, 1617–1629.

26 R. K. Harris, E. D. Becker, S. M. Cabral de Menezes, R. Goodfellow and P. Granger, *Solid State Nucl. Magn. Reson.*, 2002, **22**, 458–483.

27 S. P. Marburger, B. M. Fung and A. K. Khitrin, *J. Magn. Reson.*, 2002, **154**, 205–9.

28 R. W. Schurko, *Acc. Chem. Res.*, 2013, **46**, 1985–1995.

29 T. Giavani, K. Johannsen, C. J. H. Jacobsen, N. Blom, H. Bildsøe, J. Skibsted and H. J. Jakobsen, *Solid State Nucl. Magn. Reson.*, 2003, **24**, 218–35.

30 A. R. Hove, H. Bildsøe, J. Skibsted, M. Brorson and H. J. Jakobsen, *Inorg. Chem.*, 2006, **45**, 10873–81.

31 H. J. Jakobsen, A. R. Hove, R. G. Hazell, H. Bildsøe and J. Skibsted, *Magn. Reson. Chem.*, 2006, **44**, 348–356.

32 L. A. O'Dell, K. J. Harris and R. W. Schurko, *J. Magn. Reson.*, 2010, **203**, 156–66.

33 T. M. Rothgebs and E. Oldfield, *J. Biol. Chem.*, 1981, **256**, 6004–6009.

34 Ē. Kupče and R. Freeman, *J. Magn. Reson. Ser. A*, 1995, **115**, 273–276.

35 L. A. O'Dell, *Solid State Nucl. Magn. Reson.*, 2013, **55-56**, 28–41.

36 S. Meiboom and D. Gill, *Rev. Sci. Instrum.*, 1958, **29**, 688.

37 D. Massiot, I. Farnan, N. Gautier, D. Trumeau, P. Florian and P. J. Grandinetti, *J. Chim. Phys. Physico-Chimie Biol.*, 1995, **92**, 1847–1850.

38 J. A. Tang, J. D. Masuda, T. J. Boyle and R. W. Schurko, *ChemPhysChem*, 2006, **7**, 117–30.

39 L. A. O'Dell, A. J. Rossini and R. W. Schurko, *Chem. Phys. Lett.*, 2009, **468**, 330–335.

40 K. J. Harris, S. L. Veinberg, C. R. Mireault, A. Lupulescu, L. Frydman and R. W. Schurko, *Chem. Eur. J.*, 2013, **19**, 16469–75.

41 L. O. Andersso, M. Gourdji, L. Guibe and W. G. Proctor, *C. R. Acad. Sci.*, 1968, **267**, 803.

42 R. E. Stark, H. Van Willigen and R. G. Griffin, *J. Am. Chem. Soc.*, 1981, **103**, 2534–2539.

43 A. E. Aliev, S. E. Mann, A. S. Rahman, P. F. McMillan, F. Corà, D. Iuga, C. E. Hughes and K. D. M. Harris, *J. Phys. Chem. A*, 2011, **115**, 12201–11.

44 G. Nolze and W. Kraus, *Powder Diffr.*, 1998, **13**, 256–259.

45 P. Bertani, J. Raya and B. Bechinger, *Solid State Nucl. Magn. Reson.*, 2014, **61-62**, 15–18.

46 L. A. O'Dell and R. W. Schurko, *Chem. Phys. Lett.*, 2008, **464**, 97–102.

47 R. Bhattacharyya and L. Frydman, *J. Chem. Phys.*, 2007, **127**, 194503.

48 L. A. O'Dell and R. W. Schurko, *J. Am. Chem. Soc.*, 2009, **131**, 6658–9.

49 K. Eichele, WSolids NMR Simulation Package v1.20.15, 2011.

50 A. Bielecki and D. P. Burum, *J. Magn. Reson. Ser. A*, 1995, **116**, 215–220.

51 K. J. Harris, A. Lupulescu, B. E. G. Lucier, L. Frydman and R. W. Schurko, *J. Magn. Reson.*, 2012, **224**, 38–47.

52 S. J. Clark, M. D. Segall, C. J. Pickard, P. J. Hasnip, M. J. Probert, K. Refson and M. C. Payne, *Zeitschrift Fur Krist.*, 2005, **220**, 567–570.

53 L. F. Power, K. E. Turner and F. H. Moore, *Acta Crystallogr.*, 1976, **B32**, 11–16.

54 A. Kvick, W. M. Canning, T. F. Koetzle and G. J. B. Williams, *Acta Crystallogr. Sect. B-Structural Sci.*, 1980, **36**, 115–120.

55 A. R. Al-Karaghouli, F. E. Cole, M. S. Lehmann, C. F. Miskell, J. J. Verbist and T. F. Koetzle, *J. Chem. Phys.*, 1975, **63**, 1360.

56 Y. Iitaka, *Acta Crystallogr.*, 1958, **11**, 225–226.

57 D. G. Hughes and L. Pandey, *J. Magn. Reson.*, 1984, **56**, 425–442.

58 P. P. Man, *Solid State Nucl. Magn. Reson.*, 1992, **1**, 149–158.

59 V. V. Lemanov and S. N. Popov, *Phys. Solid State*, 1998, **40**, 991–994.

60 V. A. Drebushchak, Y. A. Kovalevskaya, I. E. Paukov and E. V. Boldyreva, *J. Therm. Anal. Calorim.*, 2003, **74**, 109–120.

61 R. A. Kumar, R. E. Vizhi, N. Vijayan and D. R. Babu, *Physica B-Condensed Matter*, 2011, **406**, 2594–2600.

62 V. Milman, B. Winkler, J. A. White, C. J. Pickard, M. C. Payne, E. V Akhmatskaya and R. H. Nobes, *Int. J. Quantum Chem.*, 2000, **77**, 895–910.

63 M. Strohmeier, D. Stueber and D. M. Grant, *J. Phys. Chem. A*, 2003, **107**, 7629–7642.

64 C. Gervais, R. Dupree, K. J. Pike, C. Bonhomme, M. Profeta, C. J. Pickard and F. Mauri, *J. Phys. Chem. A*, 2005, **109**, 6960–9.

65 R. K. Harris, A. C. Olivierit and A. C. Olivieri, *Prog. Nucl. Magn. Reson. Spectrosc.*, 1992, **24**, 435–456.

66 D. T. Edmonds, M. J. Hunt and A. L. Mackay, *J. Magn. Reson.*, 1973, **9**, 66–74.

67 D. T. Edmonds and C. P. Summers, *J. Magn. Reson.*, 1973, **12**, 134–142.

68 L. A. O'Dell and C. I. Ratcliffe, *Chem. Commun.*, 2010, **46**, 6774–6.

69 E. R. Andrew, W. S. Hinshaw and M. G. Hutchins, *J. Magn. Reson.*, 1974, **15**, 196–200.

70 E. R. Andrew, W. S. Hinshaw, M. G. Hutchins and R. O. I. Sjöblom, *Mol. Phys.*, 1976, **32**, 795–806.

71 E. R. Andrew, W. S. Hinshaw, M. G. Hutchins and R. O. I. Sjöblom, *Mol. Phys.*, 1977, **34**, 1695–1706.

72 R. W. Schurko, I. Hung and C. M. Widdifield, *Chem. Phys. Lett.*, 2003, **379**, 1–10.

73 I. Hung and Z. Gan, *J. Magn. Reson.*, 2010, **204**, 256–65.

74 K. K. Dey, J. T. Ash, N. M. Trease and P. J. Grandinetti, *J. Chem. Phys.*, 2010, **133**, 054501.

75 B. E. G. Lucier, K. E. Johnston, W. Xu, J. C. Hanson, S. D. Senanayake, S. Yao, M. W. Bourassa, M. Srebro, J. Autschbach and R. W. Schurko, *J. Am. Chem. Soc.*, 2014, **136**, 1333–51.

76 L. A. O'Dell, R. He and J. Pandohee, *CrystEngComm*, 2013, **15**, 8657.

77 L. A. O'Dell and C. I. Ratcliffe, *Chem. Phys. Lett.*, 2011, **514**, 168–173.

78 A. J. Rossini, L. Emsley and L. A. O'Dell, *Phys. Chem. Chem. Phys.*, 2014, **16**, 12890–9.

79 L. A. O'Dell, C. I. Ratcliffe, X. Kong and G. Wu, *J. Phys. Chem. A*, 2012, **116**, 1008–14.

80 R. E. Stark, R. A. Haberkorn and R. G. Griffin, *J. Chem. Phys.*, 1978, **68**, 1996.

81 R. Blinc, M. Mali, R. Osredkar, A. Prelesnik, J. Seliger and I. Zupančič, *J. Chem. Phys.*, 1972, **57**, 5087.

82 U. Werner-Zwanziger, B. Black, M. Ziegeweid and A. Pines, *Chem. Phys. Lett.*, 1993, **209**, 17–21.

83 U. Werner-Zwanziger, M. Ziegeweid, B. Black and A. Pines, *Zeitschrift Fur Naturforsch. Sect. A*, 1994, **49**, 1188–1192.

84 E. Balchin, D. J. Malcolme-Lawes, L. J. F. Poplett, M. D. Rowe, J. A. S. Smith, G. E. S. Pearce and S. A. C. Wren, *Anal. Chem.*, 2005, **77**, 3925–3930.

85 J. Seliger and V. Zagar, *Magn. Reson. Chem.*, 2008, **46**, 58–62.

86 J. Seliger and V. Zagar, *J. Phys. Chem. A*, 2010, **114**, 12083–12087.

87 J. Shinohara, K. Kobayashi, H. Sato-Akaba and H. Itozaki, *Solid State Nucl. Magn. Reson.*, 2011, **40**, 121–125.

88 J. N. Latosinska, M. Latosinska, J. Seliger and V. Zagar, *Eur. J. Pharm. Sci.*, 2012, **47**, 97–107.

89 A. J. Horsewill, *Prog. Nucl. Magn. Reson. Spectrosc.*, 1999, **35**, 359–389.

90 K. Schmidt-Rohr, A. S. Kulik, H. W. Beckham, A. Ohlemacher, U. Pawelzik, C. Boeffel and H. W. Spiess, *Macromolecules*, 1994, **27**, 4733–4745.

91 V. N. Vukotic, K. J. Harris, K. Zhu, R. W. Schurko and S. J. Loeb, *Nat. Chem.*, 2012, **4**, 456–60.

92 R. A. Kinsey, A. Kintanar and E. Oldfield, *J. Biol. Chem.*, 1981, **256**, 9028–9036.

93 L. K. Nicholson, L. E. Kay, D. M. Baldisseri, J. Arango, P. E. Young, A. Bax and D. A. Torchia, *Biochemistry*, 1992, **31**, 5253–5263.

Table 1. ^{14}N quadrupolar parameters obtained from solid-state NMR spectra and plane-wave DFT calculations and experimental $T_2^{eff}(^{14}N)$ constants.

	Experimental [a]		Plane-wave DFT (unoptimized) [b]		Plane-wave DFT (H optimized) [c]		$T_2^{eff}(^{14}N)$ (ms) [d]
	C_Q/MHz	η_Q	C_Q/MHz	η_Q	C_Q/MHz	η_Q	
α-glycine	1.19(2) [e]	0.52(2)	1.23	0.55	1.23	0.62	54(14)
β-glycine	1.26(3)	0.42(3)	1.63	0.25	1.31	0.54	12(1)
γ-glycine	1.19(4)	0.38(4)	1.28	0.42	1.26	0.41	25(4)
γ-glycine-ND_3^+	1.19(2)	0.37(2)	–	–	–	–	24(3)
glycine HCl	1.16(2)	0.17(2)	1.20	0.16	1.14	0.22	40(10)

[a] The EFG tensor is defined by three principal components ordered such that $|V_{11}| \leq |V_{22}| \leq |V_{33}|$ and $V_{11} + V_{22} + V_{33} = 0$. The quadrupolar parameters are described by $C_Q = eQV_{33}/h$ and $\eta_Q = (V_{11} - V_{22})/V_{33}$, where $0 \leq \eta_Q \leq 1.0$. [b] EFG tensor calculations without prior geometry optimization of the H atom positions. [c] EFG tensor calculations after the H atom positions were optimized. [d] ^{14}N FIDs were acquired at a transmitter frequency of 29.175 MHz, a temperature of 20 °C, and identical ^{1}H decoupling rf fields. [e] Uncertainty is reported to the last decimal place.

Figure Captions

Figure 1. ^{14}N SSNMR spectra acquired using the WURST-CPMG pulse sequence at 9.4 T for (a) α-glycine, (b) β-glycine, (c) γ-glycine and (d) glycine HCl. The vertical dashed lines mark the positions of the discontinuities (horns, shoulders, and feet) of the α-glycine powder pattern.

Figure 2. ^{14}N EFG tensor orientations in (a) α-glycine, (b) β-glycine, (c) γ-glycine and (d) glycine HCl.

Figure 3. ^{14}N WURST-CPMG powder patterns of (a) γ-glycine-ND_3^+ and (b) γ-glycine-NH_3^+ and corresponding analytical simulation (red trace, C_Q = 1.19 ± 0.02 MHz and η_Q = (0.38 ± 0.02). The vertical dashed lines mark the positions of the discontinuities (horns, shoulders and feet) of the γ-glycine-ND_3^+ powder pattern. * ^{14}N NMR signal arising from the piezoelectric response of the sample due to RF irradiation.

Figure 4. (a) Comparison of the individual sub-spectra of glycine HCl acquired with BCP and DE methods with similar acquisition parameters. The average enhancement in S/N is approximately 6.6 times for the BCP spectrum (Table S9). (b) Comparison of the entire ^{14}N SSNMR spectra of glycine HCl acquired with BCP and DE methods. Vertical dashed lines mark the edges of the "foot" discontinuity.

Figure 5. Temperature dependence of ^{14}N SSNMR signal intensity in the temperature range of −88 to +181 °C for (a) α-glycine, (b) γ-glycine, and (c) glycine HCl.

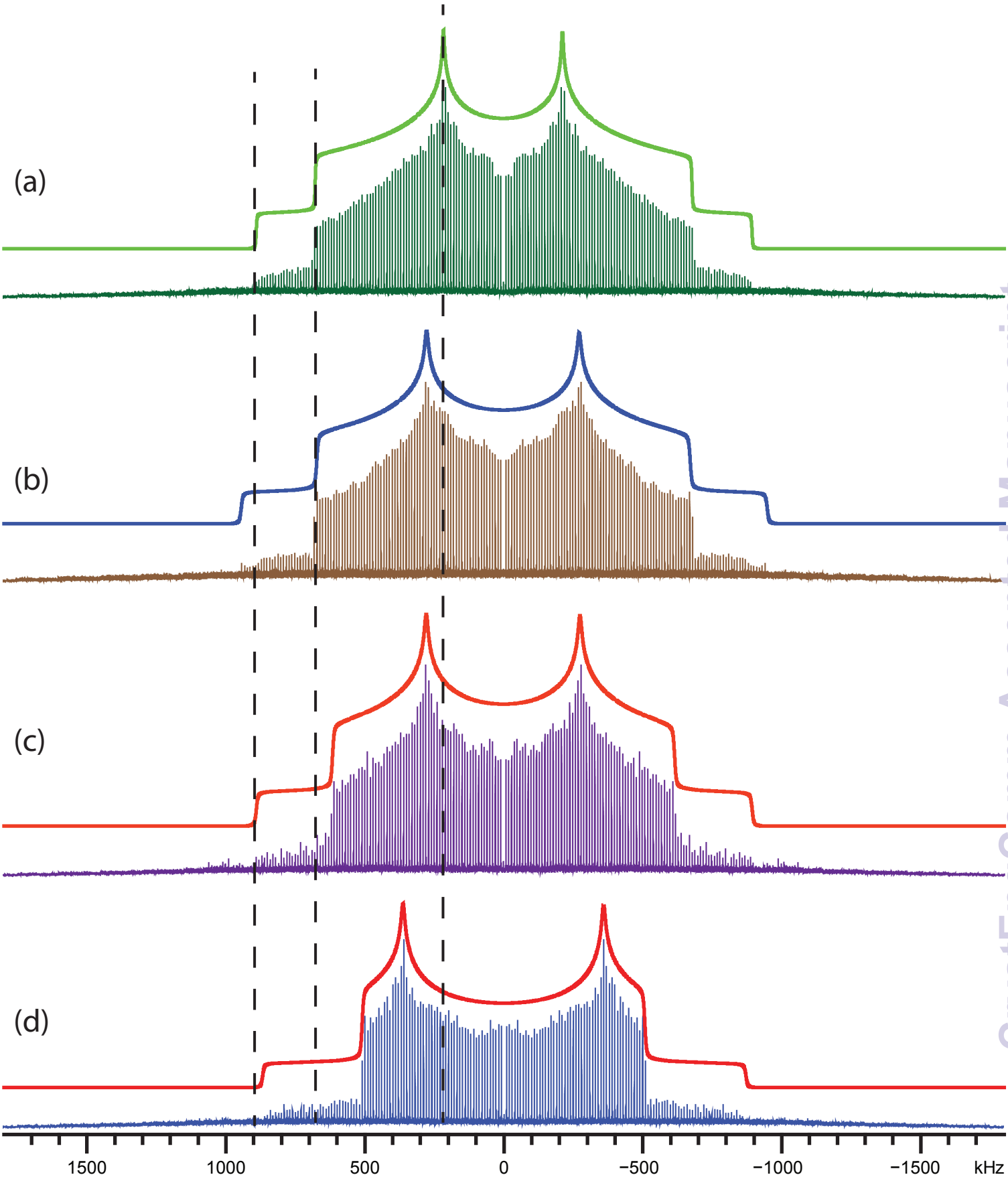

Figure 1. ^{14}N SSNMR spectra acquired using the WURST-CPMG pulse sequence at 9.4 T for (a) α-glycine, (b) β-glycine, (c) γ-glycine, and (d) glycine HCl. The vertical dashed lines mark the positions of the discontinuities (horns, shoulders, and feet) of the α-glycine powder pattern.

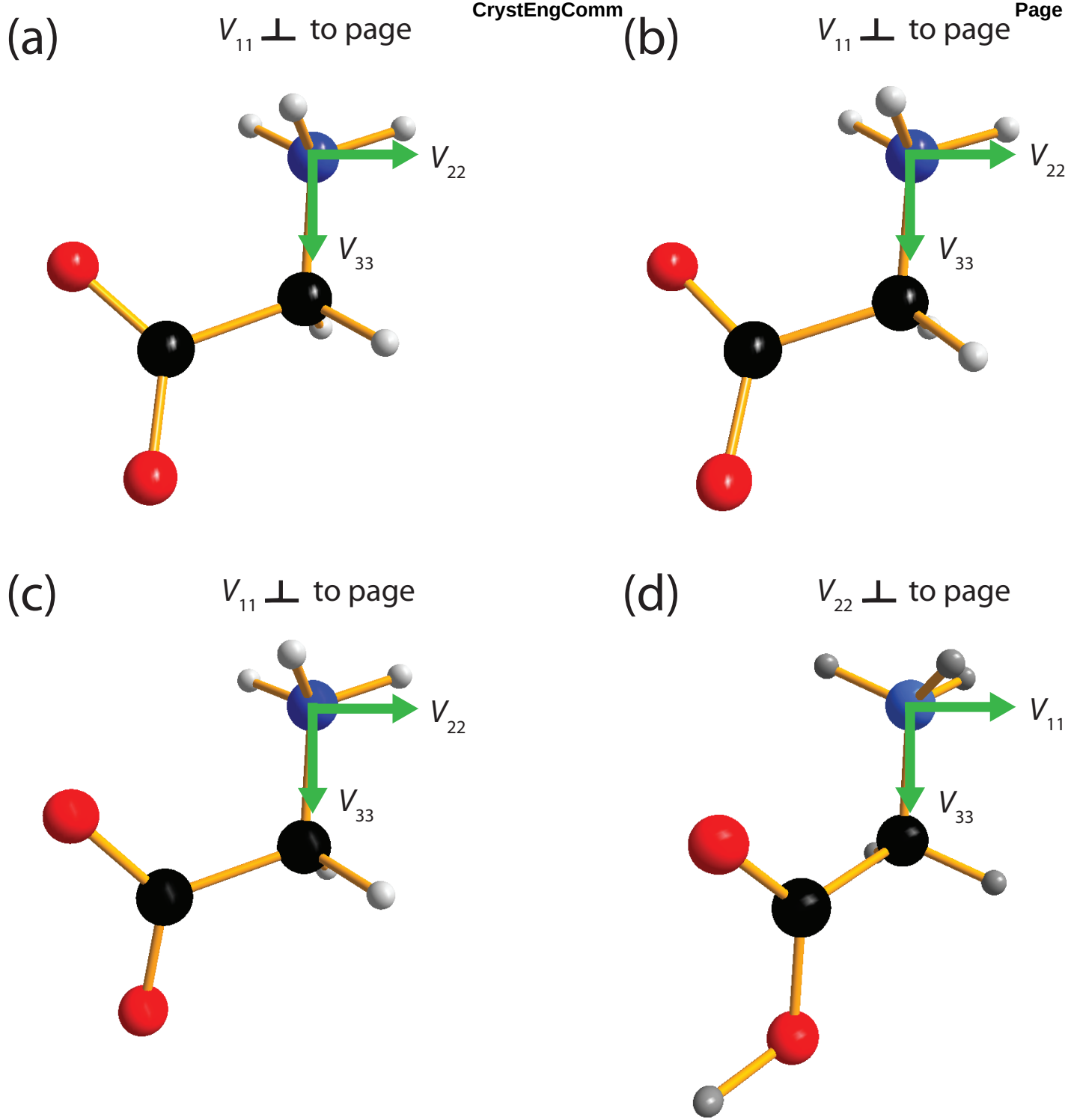

Figure 2. ^{14}N EFG tensor orientations in (a) α-glycine, (b) β-glycine, (c) γ-glycine, and (d) glycine HCl.

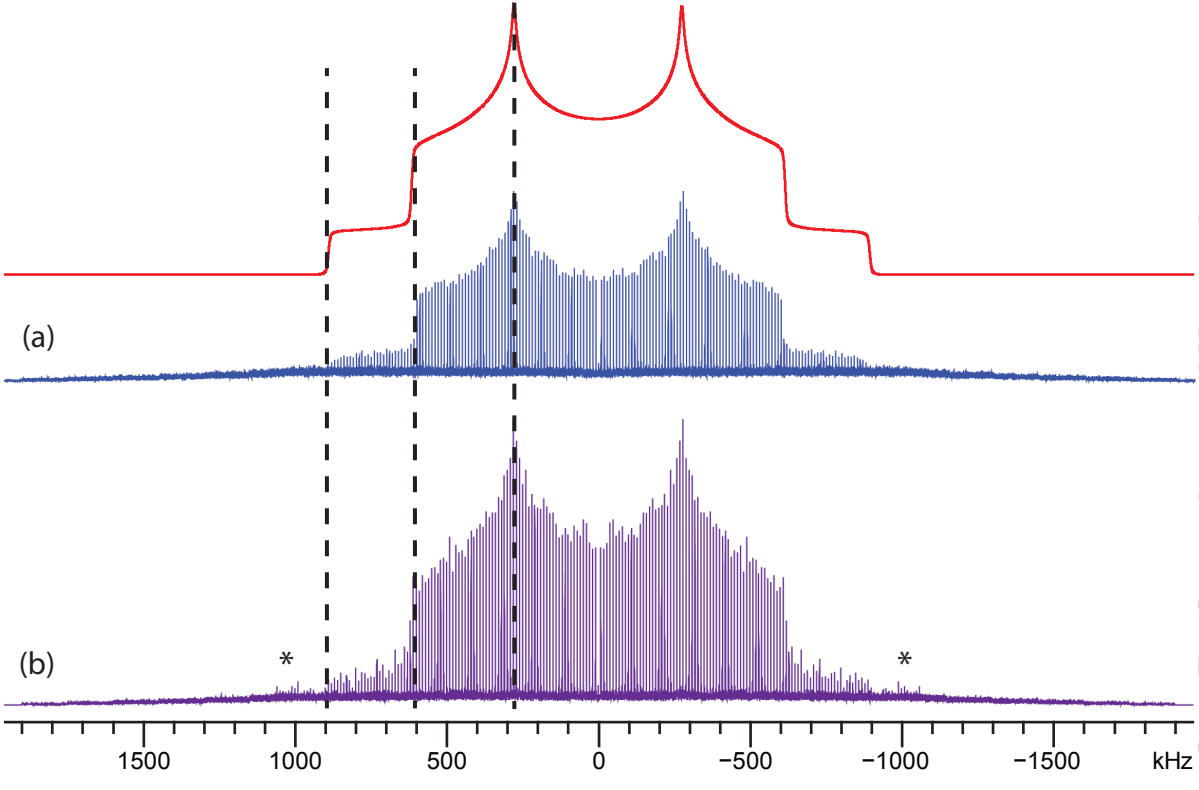

Figure 3. ^{14}N WURST-CPMG powder patterns of (a) γ-glycine-ND_3^+ and (b) γ-glycine-NH_3^+ and corresponding analytical simulation (red trace, C_Q = 1.19 ± 0.02 MHz and η_Q = 0.37 ± 0.02). The vertical dashed lines mark the positions of the discontinuities (horns, shoulders and feet) of the γ-glycine-ND_3^+ powder pattern. * ^{14}N NMR signal arising from the piezoelectric response of the sample due to RF irradiation.

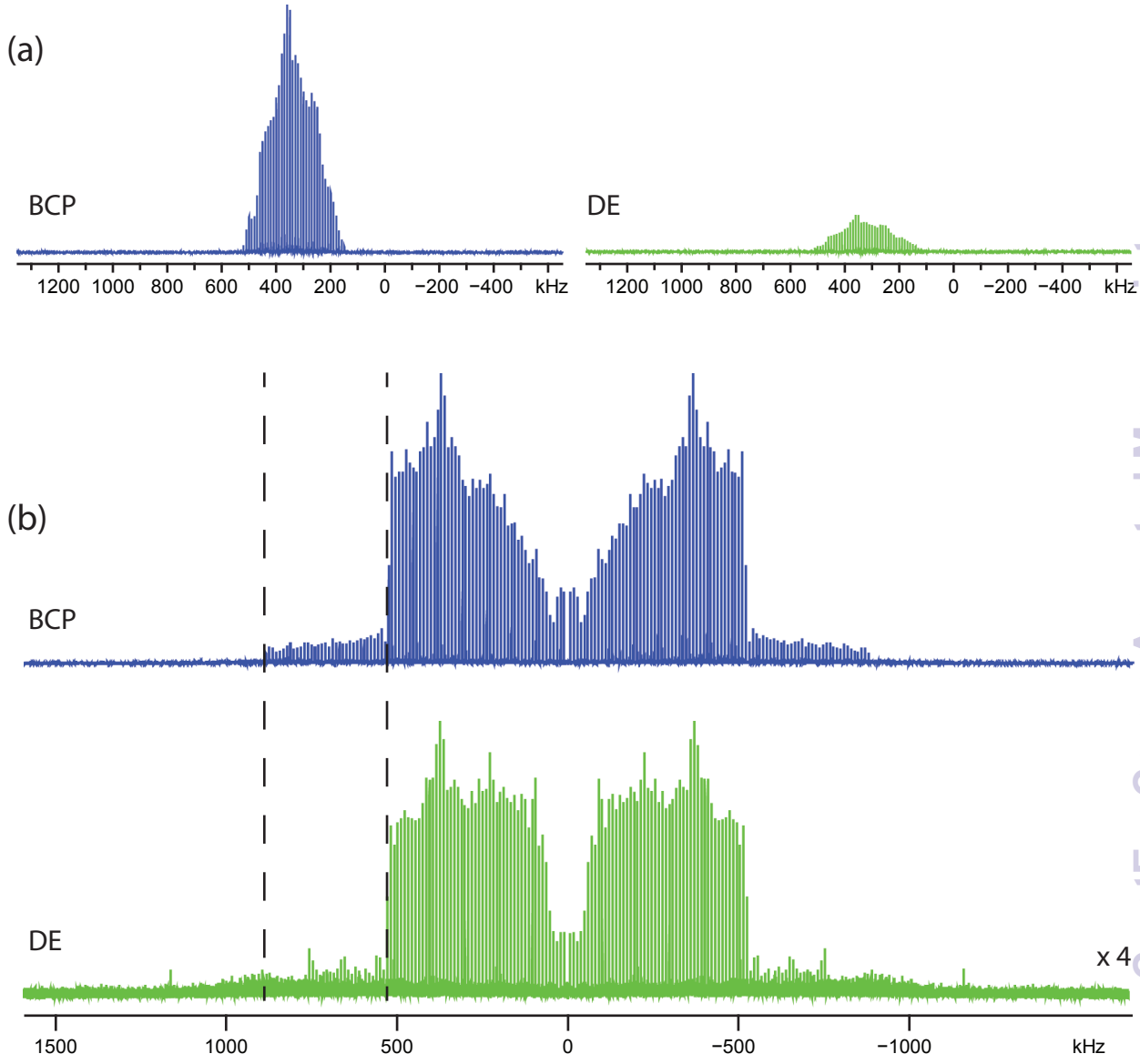

Figure 4. (a) Comparison of the individual sub-spectra of glycine HCl acquired with BCP and DE methods with similar acquisition parameters. The average enhancement in S/N is approximately 6.6 times for the BCP spectrum (Table S9). (b) Comparison of the entire ^{14}N SSNMR spectra of glycine HCl acquired with BCP and DE methods. Vertical dashed lines mark the edges of the "foot" discontinuity.

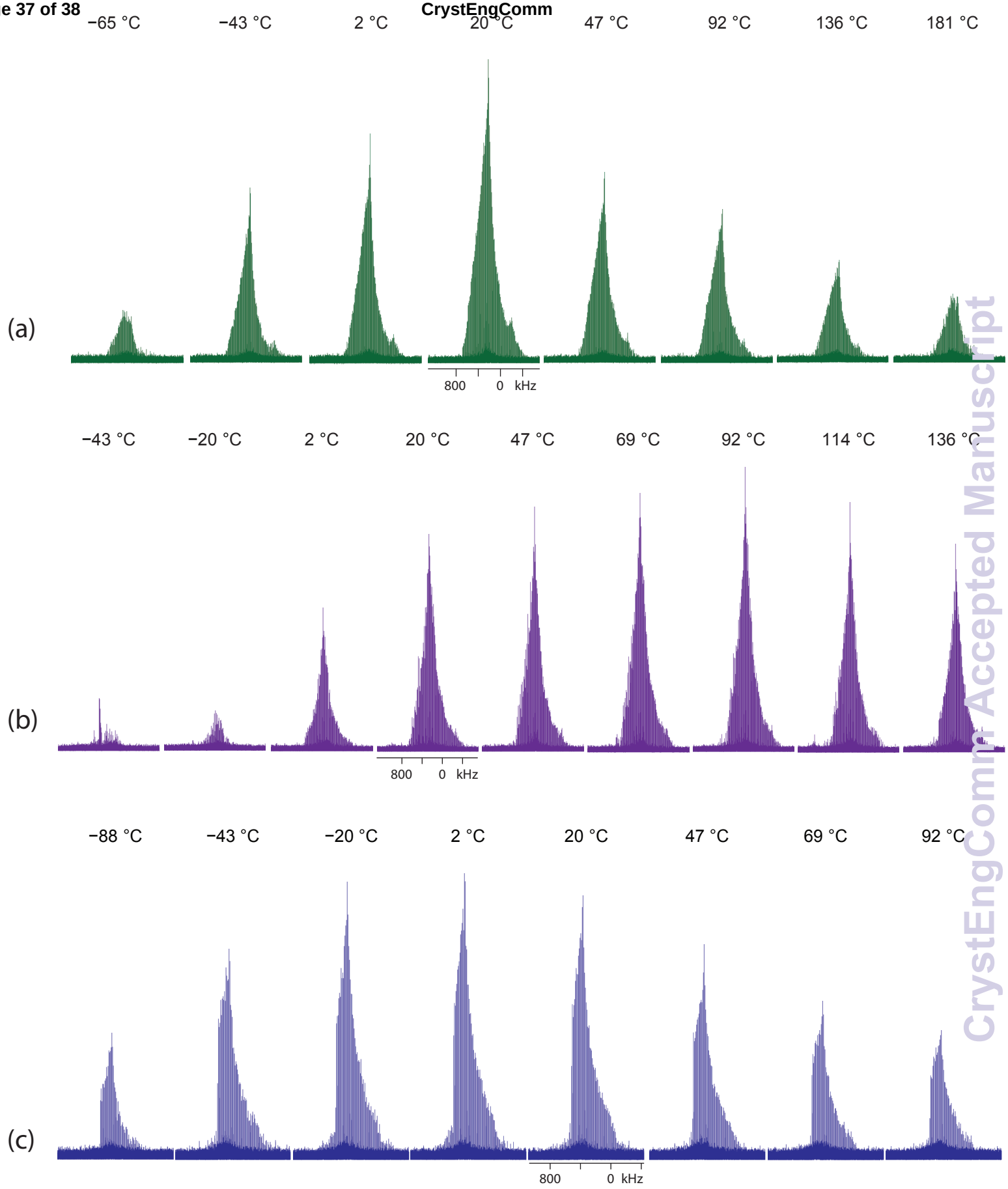

Figure 5. Temperature dependence of ^{14}N SSNMR signal intensity in the temperature range of −88 to +181 °C for (a) α-glycine, (b) γ-glycine, and (c) glycine HCl.

^{14}N solid-state NMR is useful for differentiating polymorphs and chemically distinct nitrogen-containing compounds. A case study of glycine is presented.